ACSNANO
www.acsnano.org
ARTICLE

Light-Directed Reversible Assembly of Plasmonic Nanoparticles Using Plasmon-Enhanced Thermophoresis

Linhan Lin,[†,‡,□] Xiaolei Peng,[‡,□] Mingsong Wang,[†] Leonardo Scarabelli,[§] Zhangming Mao,[∥] Luis M. Liz-Marzán,[§,⊥,#] Michael F. Becker,[‡,¶] and Yuebing Zheng*[,†,‡]

[†]Department of Mechanical Engineering, [‡]Materials Science & Engineering Program and Texas Materials Institute, and [¶]Department of Electrical and Computer Engineering, The University of Texas at Austin, Austin, Texas 78712, United States

[§]Bionanoplasmonics Laboratory, CIC biomaGUNE, Paseo de Miramón 182, 20009 Donostia, San Sebastián, Spain

[∥]Department of Engineering Science and Mechanics, The Pennsylvania State University, University Park, Pennsylvania 16802, United States

[⊥]Ikerbasque, Basque Foundation for Science, 48013 Bilbao, Spain

[#]CIBER de Bioingeniería, Biomateriales y Nanomedicina, CIBER-BBN, 20009 Donostia, San Sebastián, Spain

Supporting Information

ABSTRACT: **Reversible assembly of plasmonic nanoparticles can be used to modulate their structural, electrical, and optical properties. Common and versatile tools in nanoparticle manipulation and assembly are optical tweezers, but these require tightly focused and high-power (10−100 mW/μm^2) laser beams with precise optical alignment, which significantly hinders their applications. Here we present light-directed reversible assembly of plasmonic nanoparticles with a power intensity below 0.1 mW/μm^2. Our experiments and simulations reveal that such a low-power assembly is enabled by thermophoretic migration of nanoparticles due to the plasmon-enhanced photothermal effect and the associated enhanced local electric field over a plasmonic substrate. With software-controlled laser beams, we demonstrate parallel and dynamic manipulation of multiple nanoparticle assemblies. Interestingly, the assemblies formed over plasmonic substrates can be subsequently transported to nonplasmonic substrates. As an example application, we selected surface-enhanced Raman scattering spectroscopy, with tunable sensitivity. The advantages provided by plasmonic assembly of nanoparticles are the following: (1) low-power, reversible nanoparticle assembly, (2) applicability to nanoparticles with arbitrary morphology, and (3) use of simple optics. Our plasmon-enhanced thermophoretic technique will facilitate further development and application of dynamic nanoparticle assemblies, including biomolecular analyses in their native environment and smart drug delivery.**

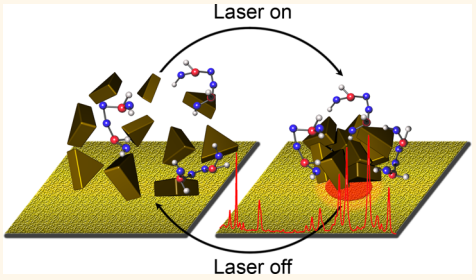

KEYWORDS: *thermophoresis, photothermal effect, surface-enhanced Raman scattering, surface plasmons, nanoparticle trapping, reversible nanoparticle assembly*

Associated with the excitation of surface plasmons, metallic nanoparticles can manipulate light at the subwavelength scale where the intense localized electromagnetic field strongly couples with nanoscale objects, leading to various light−matter interactions and applications.[1−6] The optical and electronic properties of plasmonic nanoparticles depend on the particle composition, size, and shape, as well as interparticle interactions.[7−11] Plasmonic nanoparticle assemblies that feature high particle density and small interparticle distance are important for many applications, mainly those based on the multiple electromagnetic "hot spots" that form within the assemblies.[12−15] In particular, the capability of reversibly controlling nanoparticle assemblies with external stimuli enables dynamically tunable plasmon coupling for advanced applications. Reversible assembly has been demonstrated for functionalized metal nanoparticles, driven by external stimuli such as solution pH,[15,16] local temperature,[17,18] metal-ion coordination,[19] voltage,[20] and light.[21,22]

The optical manipulation of plasmonic nanoparticles has advantages for applications such as nanofabrication,[23−28] drug delivery,[29,30] and biosensing.[31,32] Optical tweezers provide remote, real-time, and versatile manipulation of colloidal particles in solution, rendering them highly effective in the

Received: August 15, 2016
Accepted: September 16, 2016

DOI: 10.1021/acsnano.6b05486
ACS Nano XXXX, XXX, XXX−XXX

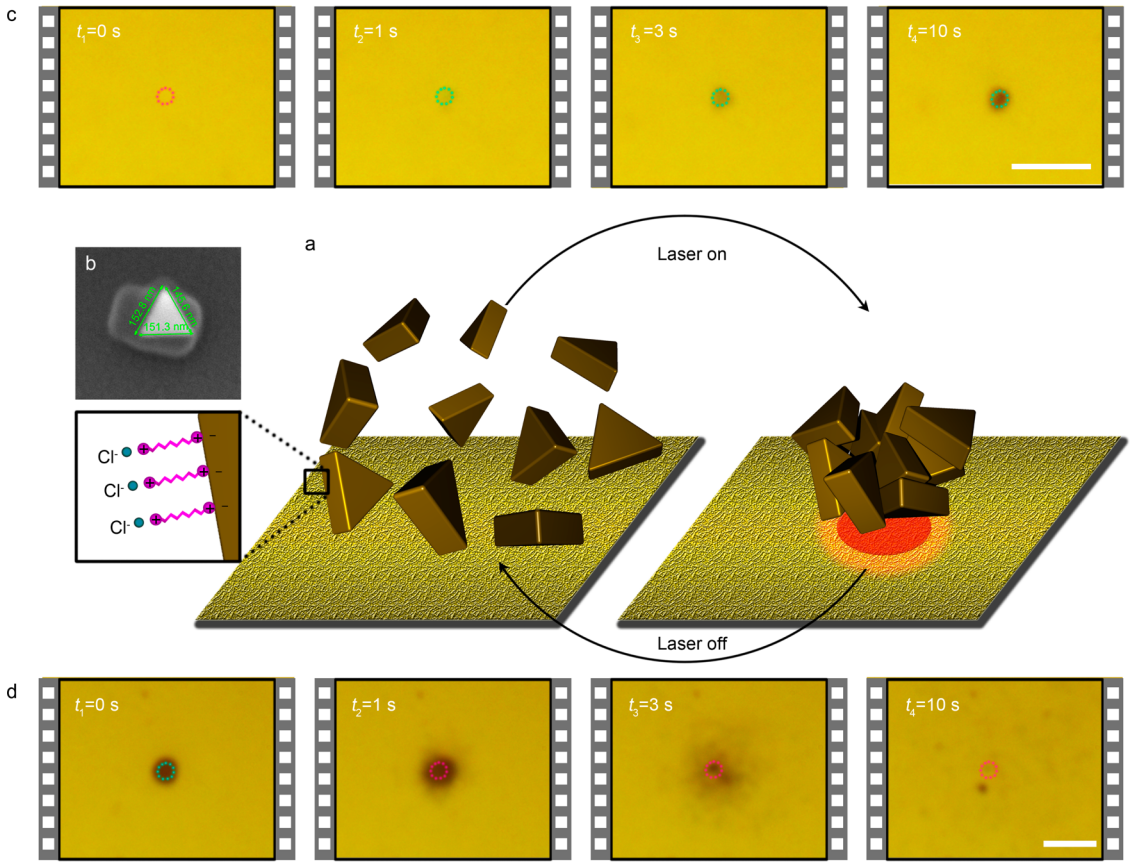

Figure 1. Light-directed reversible assembly of plasmonic nanoparticles based on plasmon-enhanced thermophoresis. (a) Schematic representation of the light-directed reversible assembly of positively charged AuNTs functionalized with CTAC. (b) Scanning electron micrograph of a single AuNT on the AuNI substrate. (c) Successive optical images during light-directed assembly of AuNTs. (d) Successive optical images showing the disassembly of an AuNT aggregate after the laser is turned off. The red and blue dotted circles indicate that the laser is off and on, respectively. Scale bars: 10 μm.

reversible assembly of plasmonic nanoparticles.[31−35] In optical tweezers, the optical gradient forces are responsible for the assembly of nanoparticles into aggregates. When the working light is turned off, the assemblies can redisperse into solution due to repulsive electrostatic interactions among the nanoparticles carrying surface charges of the same sign. However, due to the strong light scattering from plasmonic nanoparticles, optical tweezers require tightly focused laser beams of high intensity (10−100 mW/μm^2)[31−35] to generate a sufficiently strong optical gradient force for the assembly of the nanoparticles. Therefore, unexpected photochemical or thermal reactions (or damage) can occur to molecular analytes under high-power laser illumination.[36,37] Due to their enhanced local electromagnetic field and strong optical force, surface plasmon polaritons (SPPs) on metallic thin films have been harnessed to reduce the power requirement for optical assembly of nanoparticles over the film.[12] However, there are remaining limitations in exploiting plasmon-enhanced optical forces for the assembly of plasmonic nanoparticles. One limitation is that the high sensitivity of optical forces to plasmon resonances requires a strict overlap between the plasmon resonance wavelength of the nanoparticles and the working wavelength of the laser beam. This implies that a certain type of laser beam can work properly only for a limited range of nanoparticles with specific plasmon resonances. Another drawback is that, despite the rapid and even ultrafast optical response, it takes a relatively long time (~10 min) to achieve the assembly of nanoparticles in solution because near-field optical trapping on a plasmonic substrate relies on diffusion to bring the nanoparticles into the desired configuration.

On the basis of the temperature-gradient field in solution, thermophoresis has proven effective for low-energy, noninvasive trapping of particles[38−40] and biomolecules (*e.g.*, DNA).[41−43] Herein, we present a versatile optical technique that uses plasmon-enhanced thermophoresis for the efficient assembly of plasmonic nanoparticles with dynamic control over assembly size and pattern formation, at low optical power. By introducing a nonphotoresponsive cationic surfactant, namely, cetyltrimethylammonium chloride (CTAC), into the plasmonic nanoparticle suspension, we can direct the positively charged nanoparticles toward the laser spot at the interface between a plasmonic substrate and the nanoparticle dispersion. Our experiments and simulations reveal that the plasmon-enhanced temperature-gradient field and the thermally induced local electric field give rise to the delivery and assembly of plasmonic nanoparticles. By employing a holographic optical system to control the laser beam, we further achieved parallel and dynamic manipulation of multiple nanoparticle assemblies. Finally, we employed the nanoparticle assemblies with dynamically controlled electromagnetic "hot spots" for surface-enhanced Raman scattering (SERS) analysis of molecules in their native liquid environments. Using rhodamine 6G and methyl orange as model molecules, we investigated the effects of nanoparticle composition and geometry on SERS perform-

DOI: 10.1021/acsnano.6b05486
ACS Nano XXXX, XXX, XXX−XXX

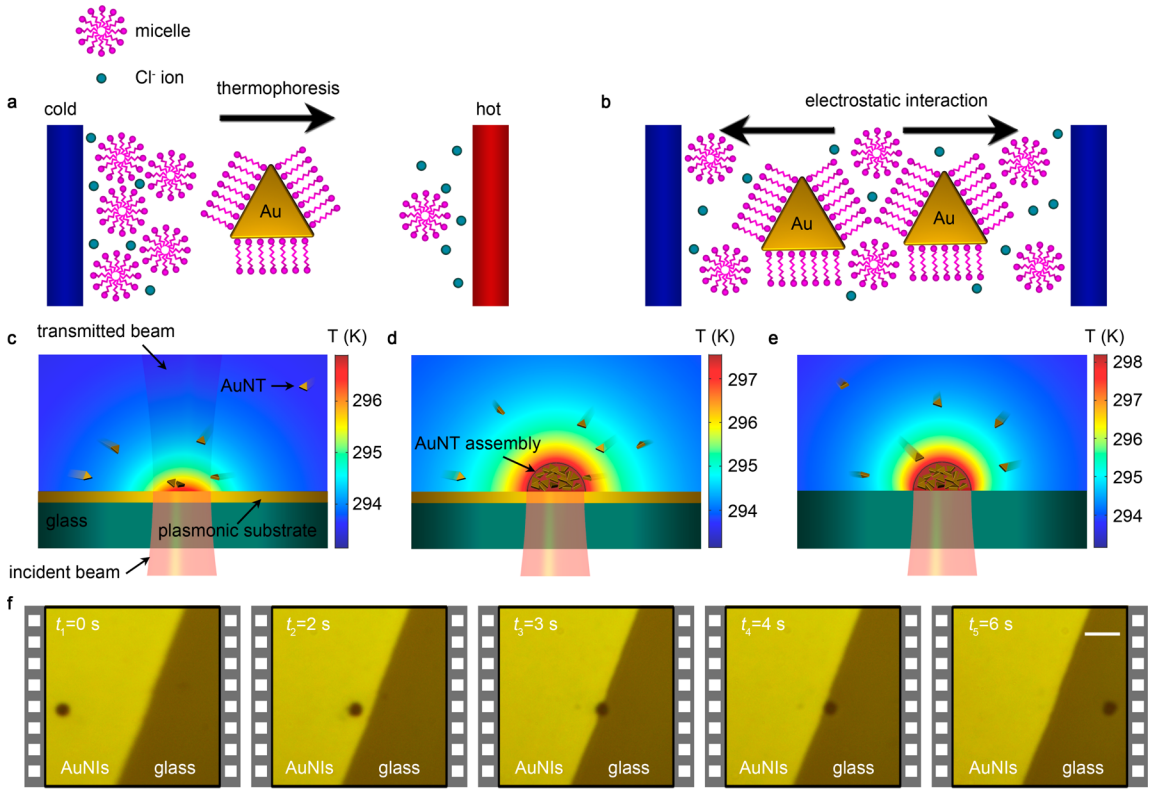

Figure 2. Working principle of light-directed reversible assembly of plasmonic nanoparticles (using AuNTs as an illustrative example). (a) Schematic illustration of the migration of a CTA^+-modified AuNT from cold to hot region in the light-induced temperature-gradient field, which is known as thermophoresis. (b) Schematic illustration of the release or redispersion of an AuNT assembly due to electrostatic repulsive interaction when the laser is off and the temperature-gradient field disappears. Simulated temperature distribution at the interface between plasmonic substrate and particle solution in a cross-sectional view: (c) before the formation of an AuNT assembly; (d) after the formation of an AuNT assembly. (e) Simulated temperature distribution at the interface between a glass substrate and nanoparticle solution in a cross-sectional view, in the presence of an AuNT assembly, indicating that the light-directed AuNT assembly can be transported from the plasmonic substrate to the glass substrate. (f) Time-evolved optical images illustrate that we can transport the AuNT assembly from a plasmonic substrate to a glass substrate by simply translating the sample stage. Scale bar: 10 μm.

ance. By taking advantage of the parallel manipulation of multiple nanoparticle assemblies, we demonstrate SERS with enhanced sensitivity.

RESULTS AND DISCUSSION

Light-Directed Reversible Assembly of Plasmonic Nanoparticles. Figure 1a illustrates the basic concept of the light-directed reversible assembly of plasmonic nanoparticles based on plasmon-enhanced thermophoresis. We selected Au nanotriangles (AuNTs) as an illustrative example, but other nanoparticles such as Au nanospheres (AuNSs) and Ag nanospheres (AgNSs) have also been used to demonstrate the generality of our technique (Figure S1). Our AuNTs feature an average side length of ~150 nm (Figure 1b, also see Figure S2) and a main localized surface plasmon resonance wavelength of 720 nm, which exhibits significantly enhanced electromagnetic fields at the AuNT tips.[44,45] The AuNTs were dispersed in an aqueous CTAC solution (10 mM). As displayed in the inset of Figure 1a, above the critical micelle concentration (cmc, 0.13−0.16 mM),[46] CTAC forms a bilayer,[47] leading to a positive and hydrophilic surface of the nanoparticle, which is surrounded by Cl^- ions in an electric double layer.

A plasmonic substrate comprising Au nanoislands (AuNIs) was employed to induce the plasmon-enhanced photothermal effect (see Figure S3), which allows us to use a low optical power to create an appropriate temperature-gradient field for the thermophoretic assembly of nanoparticles. It should be noted that the AuNIs substrate can be easily fabricated by deposition of an Au thin film followed by postannealing (see Methods for details). When the plasmonic substrate is illuminated with a low power laser beam, the plasmonic heating of the AuNIs on the substrate increases the temperature of the surrounding environment. Thermophoresis then arises from the temperature gradient and enables the rapid formation of AuNT assemblies at the laser spot, in the vicinity of the substrate−solution interface (Figure 1c). Successive optical images of the light-directed assembly process are shown in Figure 1c, revealing the formation of a stable AuNT assembly at t_4 = 10 s. Importantly, the AuNTs can redisperse into the solution once the laser is turned off (Figure 1d). The reversible assembly process is also shown in Supporting Movies 1 and 2.

The assembly of AuNTs is caused by particle migration in the thermally induced local electric field, i.e. thermoelectric effect.[42,48] As illustrated in Figure 2a, a light-induced local temperature gradient imposes a nonuniform concentration of CTAC micelles, due to the thermal response of the positively charged micelles. The positive surface of CTAC micelles is surrounded by Cl^- ions, giving rise to an electric double layer. Treating these positive micelles as macroions, we obtain the Debye screening length λ_{DH}:

DOI: 10.1021/acsnano.6b05486
ACS Nano XXXX, XXX, XXX−XXX

$$\lambda_{DH} = \left(\frac{\varepsilon k_B T}{2Ie^2}\right)^{1/2} \quad (1)$$

where ε is the dielectric constant of the liquid, k_B is Boltzmann's constant, T is the absolute temperature, e is the electron charge, and I is the ionic strength. In the absence of added salt in the solvent, the ionic strength I is dominated by the total surfactant concentration, c, and the cmc. In the presence of the temperature-gradient field, the asymmetric ion distribution in the electric double layer exerts a pressure and causes slip flow of the liquid, which can be described with the excess enthalpy h within an interaction length λ:[49]

$$v_s = D_T^{mic}\nabla T = -\frac{1}{\eta}\int_0^\infty dz\left[zh(z)\frac{\nabla T}{T}\right] \quad (2)$$

where D_T^{mic} denotes the thermal diffusion coefficient of the micelles. Considering the Debye–Hückel approximation $h = -1/2\varepsilon(\zeta/\lambda)^2 e^{-2z/\lambda}$, where ζ is the surface potential, the thermal diffusion coefficient is

$$D_T^{mic} = \frac{\varepsilon\zeta^2}{8\eta T} \quad (3)$$

where η is the viscosity of the liquid. A positive D_T^{mic} indicates that the liquid flow moves from a cold to a hot region, while in the laboratory frame, the micelles move in the opposite direction, *i.e.*, from a hot to a cold region, which is independent of the sign of ζ. The highly charged micelles give rise to the surface potential, and it is estimated that $D_T^{mic} \approx 10^{-11}$ m^2/(K s) for CTAC micelles at a concentration of 10 mM. Even though Cl^- ions have a higher mass diffusion coefficient (2×10^{-9} m^2/s)[42] than the micelles (6×10^{-10} m^2/s),[50] the extremely low Soret coefficient of Cl^- ions (7×10^{-4} 1/K) leads to a lower $D_T^{Cl^-} \approx 10^{-12}$ m^2/(K s).

The higher D_T^{mic} drives the positive CTAC micelles toward the cold region quickly and leads to the separation between negative and positive ions, thereby generating a temperature-dependent local electrostatic potential $\left(\frac{\nabla T}{T}\right)\psi_0$, as illustrated in Figure 2a. This exerts an electric force on the positive AuNTs and drives migration of the particles toward the hot region (*i.e.*, the laser beam spot) to form the assembly. According to the Helmholtz–Smoluchowski electrophoretic mobility $\varepsilon\xi/\eta$, the thermal diffusion coefficient of the AuNTs can be calculated using[51]

$$D_T^{NP} = \frac{\varepsilon\zeta^{NP}\psi_0}{\eta T} \quad (4)$$

We can estimate $D_T^{NP} \approx 10^{-12}$ m^2/(K s), which agrees with the order of magnitude of the measured trapping velocity of the AuNTs (several micrometers per second).

When the nanoparticles are in close contact within the assembly, the van der Waals attraction becomes strong enough to stabilize the assembly. However, the electrostatic repulsive force between the positive CTA^+ molecules on the nanoparticle surfaces has a negative effect on the assembly stability, which can lead to the disassembly process. Therefore, a balance among the thermally induced electric force, van der Waals attraction, and electrostatic repulsive force enables the reversible assembly of the nanoparticles. When the laser is turned off, the temperature-gradient field disappears and the nanoparticles in the aggregate are separated from each other due to the electrostatic repulsive force (Figure 2b), leading to the redispersion of the nanoparticles and thus the disassembly of the aggregates.

To estimate the plasmon-enhanced photothermal effect and its role in the assembly of the plasmonic nanoparticles, we simulated the temperature-gradient profiles at the substrate–solution interface upon illumination with a laser beam, as displayed in Figure 2c–e. When a 532 nm laser beam (power: 0.1 mW, diameter: 2 μm) is incident on the plasmonic substrate, a moderate temperature gradient of ~0.6 K/μm is obtained on top of the substrate. The rapid migration of the AuNTs to the hot region at the interface between the substrate and solution leads to growth of the aggregate. It should be noted that the AuNTs assembled on top of the plasmonic substrate absorb light that would otherwise be transmitted through the substrate, which further increases the photothermal effect and the temperature gradient. As displayed in Figure 2d, when an AuNT assembly with a diameter of 2 μm forms on top of the plasmonic substrate, the transmitted light through the substrate is completely absorbed by the AuNT assembly, leading to a temperature gradient of ~0.7 K/μm.

The optical power density used herein (~0.03 mW/μm^2) is at least 3 orders of magnitude lower than that used in optical tweezers for nanoparticle assembly.[31,32,35] We find that an optimal optical power is required to create the stable assembly of nanoparticles with plasmon-enhanced thermophoresis. A too low optical power (<0.01 mW/μm^2) cannot create a sufficiently strong local electric field to trap the nanoparticles as required for the assembly process. However, a too high optical power (>0.15 mW/μm^2) will induce strong thermal convection and Brownian motion of the plasmonic nanoparticles, causing instability of the particle assembly (Figure S4).

Further, we find that, while the AuNIs-based plasmonic substrate is required to initiate the light-directed assembly of nanoparticles *via* the plasmon-enhanced photothermal effect, it is not essential to maintain and to dynamically manipulate the assemblies once formed. The nanoparticle assembly itself becomes a heating source to maintain the force balance. As shown in Figure 2e, the light absorption by an AuNT assembly on a glass substrate can generate a temperature gradient of ~0.8 K/μm, which is even higher than that on the plasmonic substrate. Unlike the plasmonic substrate where the incident light is partially reflected at the interface between AuNIs and a glass substrate, the glass substrate exhibits a significantly reduced reflection loss. The self-sustainability of the heating source sets the foundation for delivering a stable nanoparticle assembly over a nonplasmonic substrate. As experimentally demonstrated in Figure 2f (also see Supporting Movie 3), a stable AuNT assembly with a diameter of 4 μm was generated over the plasmonic substrate at t_1 and transported across the AuNI/glass boundary at t_2–t_4 and over the glass substrate at t_5 (6 s). The transport was achieved by simply translating the sample stage.

We exclude the contribution of optical tweezing effect to our light-directed assembly of nanoparticles. Our experiments reveal that light-directed assembly occurred only on top of the plasmonic substrate. Focusing the same laser beam at the interface of a glass substrate and the nanoparticle dispersion could not initiate nanoparticle assembly, indicating that the optical force from the focused laser beam cannot trap and assemble the nanoparticles in this case. In fact, the transmitted laser beam through the substrate exerts a scattering force on the nanoparticle, pushing it away from the substrate and thus

DOI: 10.1021/acsnano.6b05486
ACS Nano XXXX, XXX, XXX–XXX

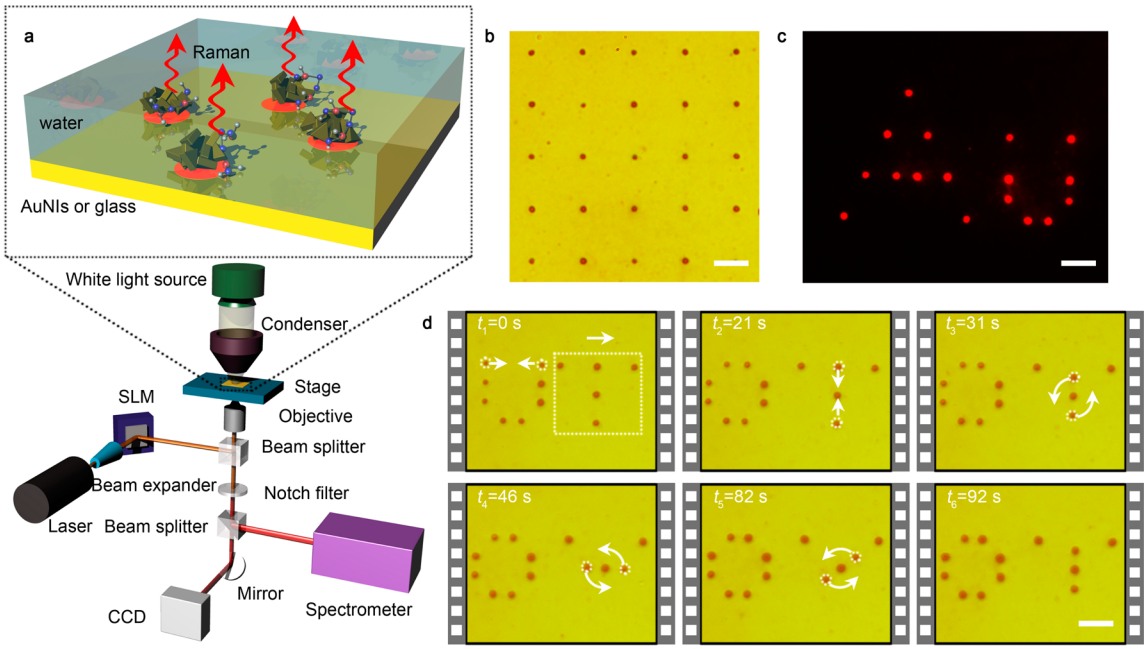

Figure 3. Parallel and dynamic manipulation of multiple nanoparticle assemblies. (a) Schematics of the optical setup for nanoparticle assembly manipulation and "multiplex" *in situ* SERS. (b) Optical image of 25 AuNT assemblies in a 5 × 5 square array. (c) Dark-field optical image of 17 AuNT assemblies in an "Au" pattern. (d) Time-evolved optical images of dynamic manipulation of selected AuNT assemblies to transform the pattern. Scale bars: 10 μm. The total power of the 532 nm working laser beam is 7.9, 3.6, and 3.6 mW for parallel manipulation in (b), (c), and (d), respectively. The diameter of individual laser beams for single assemblies is 2 μm.

preventing trapping and assembly. One may argue that the plasmon-enhanced optical force on the plasmonic substrate can improve the trapping and assembling capability of nanoparticles. However, the AuNI plasmonic substrate exhibits weak electromagnetic field enhancement under laser illumination, which is far from the condition for the maximum optical gradient force that is strong enough for particle assembly.[52] To further verify our hypothesis, we irradiated the same laser beam at the interface of AuNI substrate and nanoparticle suspensions without CTAC surfactant (AuNSs stabilized in PBS solution). As expected, no assembly of the nanoparticles occurred due to the absence of the thermoelectric effect.

Parallel and Dynamic Manipulation of Nanoparticle Assemblies. Taking advantage of versatile light management *via* holographic optics, we achieved efficient manipulation of multiple nanoparticle assemblies. The optical setup is displayed schematically in Figure 3a. A spatial light modulator (SLM) was used to dynamically control the laser beam in an arbitrary manner. Desired optical patterns on the plasmonic substrate were obtained by focusing an expanded laser beam that is modulated by the SLM onto the substrate.

Through engineering the optical patterns on the plasmonic substrate, we demonstrate the simultaneous generation of 25 AuNT assemblies in a 5 × 5 square array (Figure 3b). Another example is 17 AuNT assemblies in an "Au" pattern (Figure 3c). Despite an optical power variation of ∼20% among the different laser beams generated by the SLM, which is caused by the design algorithm, we can still generate multiple AuNT assemblies with high uniformity and stability. Furthermore, we demonstrate the dynamic manipulation of the AuNT assemblies, as shown in Figure 3d (see Supporting Movie 4 for real-time manipulation). In the demonstration, we generated 13 AuNT assemblies in a "UT" pattern at t_1. A series of transport processes of selected assemblies is implemented to transform the pattern, as shown from t_1 to t_6 in Figure 3d.

Since the formation of nanoparticle assemblies relies only on the photothermal effect from the plasmonic substrate and the CTAC surfactant, we expect that our technique is applicable to metallic nanoparticles with different materials, sizes, and shapes. Along this line, we demonstrate the light-directed assembly of metal nanoparticles of different compositions, sizes, and shapes (Figure S5), as discussed below. This versatile manipulation of the nanoparticle assemblies can be harnessed as dynamic lithography to form arbitrary patterns of dispersed nanoparticles at solid−liquid interfaces. With their reversible characteristics, the lithographic patterns can be "erased" and "rewritten" repeatedly. The minimum size of a single nanoparticle assembly can reach ∼1 μm with our current optical setup, which is determined by the size of the laser spot. The light-directed dynamic manipulation of multiple nanoparticle assemblies also allows us to develop an *in situ* SERS platform with enhanced sensitivity, as discussed below.

***In Situ* SERS.** Exploiting the plasmon-enhanced electromagnetic field at plasmonic nanostructures, SERS is an advanced analytical technique that can detect molecules with a sensitivity down to the single-molecule level.[53−56] A number of approaches have been implemented to enhance the localized electromagnetic field and improve the SERS sensitivity, including tailoring the particle shape[44,57,58] and inducing near-field coupling.[14,59−63] The integration of optical tweezers with SERS (also known as SERS tweezers) is applied for analyzing biomolecules in their native environments and developing optofluidics-based lab-on-a-chip systems.[31−34] However, the high optical power required for nanoparticle manipulation in optical tweezers can potentially damage the biomolecules,[13] which limits the applications of SERS tweezers.

With low-power operation and reversible assembly of plasmonic nanoparticles, our plasmon-enhanced thermopho-

DOI: 10.1021/acsnano.6b05486
ACS Nano XXXX, XXX, XXX−XXX

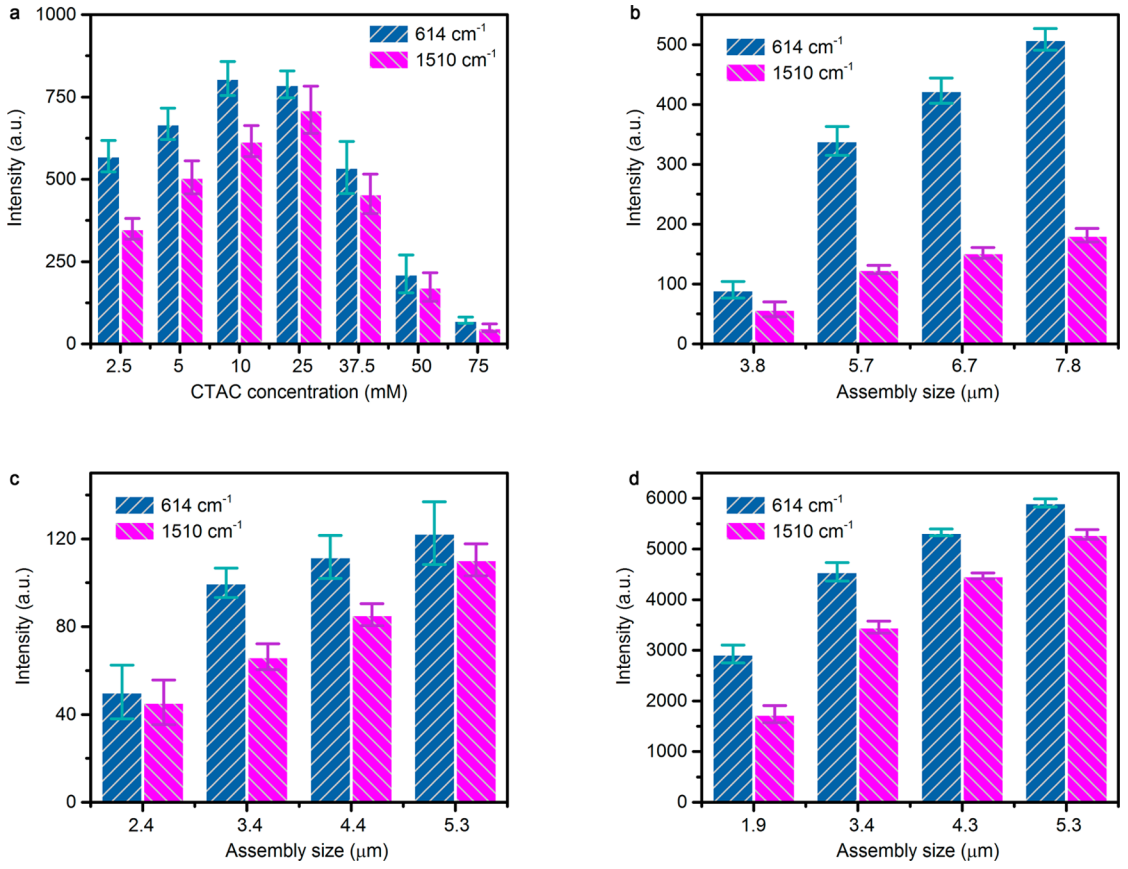

Figure 4. Parametric study of SERS of rhodamine 6G on plasmonic nanoparticle assemblies. (a) SERS intensities of 614 and 1510 cm^{-1} modes as a function of CTAC concentration in the AuNS solution. The size of AuNS assemblies over the plasmonic substrate was maintained at 4.0 ± 0.2 μm. (b) Assembly size-dependent SERS intensities of the modes at 614 and 1510 cm^{-1}, based on AuNT assemblies over a plasmonic substrate. (c) Assembly size-dependent SERS intensities of the modes at 614 and 1510 cm^{-1}, based on AuNT assemblies over a glass substrate. (d) Assembly size-dependent SERS intensities of the modes at 614 and 1510 cm^{-1}, based on AgNS assemblies over a plasmonic substrate. A 660 nm laser beam with a power of 0.27 mW and a diameter of 2 μm was used for both nanoparticle assembly and SERS measurements. The rhodamine 6G concentration was 1 mM. Acquisition times were 10 s in (a) and 1 s in (b)−(d).

retic technique has advantages for use in SERS tweezers, as demonstrated herein by *in situ* molecular sensing. SERS measurements can also be applied to monitor the dynamics of light-directed nanoparticle assembly. Considering the critical role of CTAC in the assembly of nanoparticles, we investigated the effects of CTAC concentration on the performance of SERS based on our nanoparticle assemblies. For this study, we used AuNS assemblies (see Figure S5) as the SERS substrates and rhodamine 6G as the targeted molecules. A single laser beam was used for both inducing nanoparticle assembly and Raman excitation. A typical SERS spectrum of rhodamine 6G recorded from a single AuNS assembly (CTAC concentration: 10 mM) is shown in Figure S6. However, as we show in Figure 4a, SERS intensities at 614 cm^{-1} (C−C−C ring in-plane bending mode) and 1510 cm^{-1} (aromatic C−C stretching mode)[64] are highly sensitive to CTAC concentration. Specifically, both modes experience an increase and then a decrease in intensity when CTAC concentration was increased from 2.5 mM to 75 mM. An optimal CTAC concentration of 10−25 mM was identified for the highest SERS intensities, which is likely due to the opposite trend of two different parameters with the concentration of CTAC molecules. On one hand, the increased concentration of CTAC molecules leads to an enhanced thermally induced electric field, which generates stable nanoparticle assemblies with stronger localized electromagnetic field and more intense SERS signals. On the other hand, the increased concentration of CTAC hinders the adsorption of the targeted molecules on the plasmonic nanoparticles, leading to weaker Raman enhancement.

We can further exploit the near-field coupling between the plasmonic substrates and the plasmonic nanoparticle assemblies to improve the SERS performance. Figure 4b and c summarize the dependence of the SERS intensities (of modes at 614 and 1510 cm^{-1}) on the size of AuNT assemblies over a plasmonic substrate and a glass substrate, respectively. In both cases, the SERS intensity increases with the size of the aggregate, which can be attributed to the increased number of plasmonic "hot spots" and targeted molecules in the larger assemblies. A significant improvement of SERS performance is observed for assemblies over the plasmonic substrate due to assembly substrate plasmon coupling. In addition, we notice that the SERS sensitivity of AuNT assemblies is almost an order of magnitude higher than that of AuNS assemblies because the AuNTs exhibit significantly enhanced electromagnetic fields at their tips. It should be noted that exposure time in Figure 4a was 10-fold longer than that in Figure 4b and c.

We extended our technique to reversibly assemble AgNSs (Figure S5) and then applied the AgNS assemblies for SERS detection of rhodamine 6G. Figure 4d shows the dependence on assembly size of the SERS intensities for two modes (614

DOI: 10.1021/acsnano.6b05486
ACS Nano XXXX, XXX, XXX−XXX

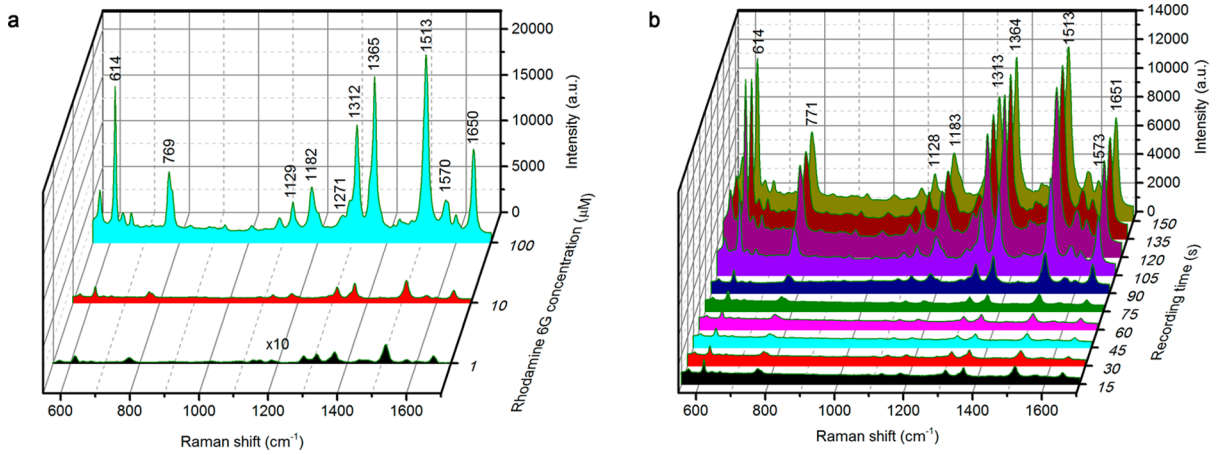

Figure 5. (a) SERS spectra recorded from single AgNS assemblies over a plasmonic substrate, for different concentrations of rhodamine 6G. The assembly size is 5.0 ± 0.2 μm. (b) Time-resolved SERS spectra of rhodamine 6G (10 μM) based on a single AgNS assembly during the solvent evaporation. At 0 s, the assembly is immersed in the solvent. At 135 s, the assembly is 100% dry. A 660 nm laser beam with a diameter of 2 μm and a power of 0.27 mW (a) and 0.32 mW (b) was used for both nanoparticle assembly and SERS measurements. Acquisition times were 10 s (a) and 15 s (b).

and 1510 cm^{-1}). AgNSs with a diameter of ~100 nm exhibit a plasmon resonance wavelength of 480 nm (Figure S1), which is much shorter than the wavelength of our working laser beam (660 nm). Compared with AuNTs, AgNSs exhibit smaller maximum assembly size because of the faster Brownian motion of the smaller AgNSs and the weaker photothermal effect at the AgNS assembly. Still, AgNS assemblies exhibit significantly higher SERS efficiency than AuNT assemblies, with an enhancement factor 1 order of magnitude higher. Our observation is consistent with previous studies regarding the superior SERS performance of Ag nanoparticles.[65]

We additionally evaluated the ultimate SERS sensitivity by studying the dependence of SERS signals on the concentration of rhodamine 6G, using a single AgNS assembly as SERS substrate. As shown in Figure 5a, we obtained a detection limit of ~1 μM for an acquisition time of 10 s. We subsequently developed two strategies to further enhance the SERS sensitivity. The first strategy comprised drying the nanoparticle assemblies. The hydrophobic interactions between the CTA^+ tails maintain the CTA^+ double layers, which exert the electrostatic repulsive force on the nanoparticles to maintain a certain interparticle distance. Solvent removal would eliminate the hydrophobic interaction and damage the CTA^+ double layers, thereby reducing the repulsive force. Therefore, we expected that a dried nanoparticle assembly would become more compact, with smaller interparticle distances due to stronger van der Waals interactions and weaker electrostatic repulsive forces. The more compact assemblies can thus enhance the local electromagnetic field at "hot spots", and the Raman signals of the molecules would be further amplified. Figure 5b shows the time-resolved SERS spectra of rhodamine 6G recorded from a single AgNS assembly during solvent evaporation, indeed showing an increase of the signal. The second strategy was based on using multiple nanoparticle assemblies for SERS. To demonstrate this concept, we generated one, two, and three nanoparticle assemblies for the SERS detection of rhodamine 6G. As shown in Figure S7, the SERS signals increase with the number of assemblies. Finally, we have extended assembly-based SERS for detection of methyl orange, with a detection limit of 5 μM using a single AgNS assembly (see Figure S8).

CONCLUSIONS

We have developed a general method for light-directed reversible assembly of plasmonic nanoparticles based on plasmon-enhanced thermophoresis. The non-photoresponsive CTAC surfactant forms a double layer to create a hydrophilic and positive nanoparticle surface. Such surface-functionalized nanoparticles can be driven into the hot region on top of a plasmonic substrate, under the plasmon-enhanced temperature-gradient field. The coordinated action from thermophoresis-induced electric force, electrostatic repulsive force, and van der Waals attraction enables the reversible assembly of plasmonic nanoparticles regardless of their composition, size, and shape. Using a holographic optical system, we achieved parallel manipulation of multiple particle assemblies. Compared with optical tweezers, our thermophoretic method features lower optical power and higher assembly efficiency, with simpler optics. Furthermore, we demonstrate that these plasmonic nanoparticle assemblies can be applied for SERS with enhanced sensitivity. With low power and parallel operation, reversible nanoparticle assembly, and general applicability to arbitrary nanoparticles, our technique will find applications in particle trapping, manipulation, patterning, and biosensing.

METHODS

Preparation of AuNIs as Plasmonic Substrates. A 4.5 nm Au thin film was deposited on a glass coverslip by thermal evaporation (Denton thermal evaporator) at a base pressure of 9×10^{-6} Torr. The Au thin film was annealed in air at 550 °C for 2 h to obtain the AuNIs on the coverslip.

Preparation of Plasmonic Nanoparticle Dispersions. AuNTs in a CTAC solution (10 mM in DI water) was prepared by previously reported synthesis protocols.[20] A 60 μL as-prepared AuNT solution was centrifuged for 10 min (4500 rpm), and the AuNTs were redispersed in 20 μL of CTAC solution (10 mM) by sonication for 10 min. The 100 nm AuNSs in PBS (0.1 mM) were purchased from Sigma–Aldrich. A 60 μL amount of as-purchased AuNS solution (0.0389 mg/mL) was centrifuged for 10 min (4500 rpm), and the AuNSs were redispersed in 20 μL of CTAC solutions with concentrations of 5, 10, 20, 50, 75, 100, and 150 mM, respectively. The 100 nm AgNSs (0.02 mg/mL) with citrate-functionalized surfaces were purchased from nanoComposix. A 200 μL amount of as-purchased AgNS solution was centrifuged for 10 min (4500 rpm), and

DOI: 10.1021/acsnano.6b05486
ACS Nano XXXX, XXX, XXX–XXX

the AgNSs were redispersed in 20 μL of CTAC solution (20 mM) by sonication for 10 min.

Preparation of Solutions for SERS. As-prepared rhodamine 6G solutions (2 mM) were diluted to a series of concentrations of 200, 20, and 2 μM. As-prepared methyl orange solutions (10 mM) were diluted to a series of concentrations of 1 mM, 100 μM, and 10 μM. The different solutions of molecular analytes were mixed with plasmonic nanoparticle solutions of various concentrations in a 1:1 ratio. The mixtures were sonicated for 5 min. Mixed solutions of 10 μL were sandwiched between the AuNIs (as a plasmonic substrate) and a coverslip with a 120 μm spacer for SERS measurements.

Light-Directed Assembly of Plasmonic Nanoparticles. To optically assemble plasmonic nanoparticles, a 532 nm diode-pumped solid-state (DPSS) laser (Coherent, Genesis MX STM-1 W) was expanded with a 5× beam expander and focused onto the plasmonic substrate through a 60× objective (Newport, NA 0.85). The *in situ* optical imaging was achieved through a customized upright Nikon microscope with 10× (NA: 0.30) and 100× (NA: 0.90) objectives. A Fourier transform hologram setup was used to create multiple laser spots. Multiple nanoparticle assemblies were achieved using an SLM (Boulder Nonlinear Systems, model P512), two relay lenses (both of focal length 20 cm), and a 50× long working distance objective (Mitutoyo, NA: 0.55).

Optical Characterization. Optical transmission spectra of plasmonic substrates and plasmonic nanoparticle solutions were taken using an Ocean Optics spectrometer (HR4000CG-UV-NIR). Raman spectra were recorded with an Andor Shamrock 303i spectrograph (grating: 1199 l/mm and slit width: 45 μm) and a Newton EMCCD integrated with an inverted Nikon microscope. The background of the Raman spectra was removed by subtracting a five-order polynomial. For *in situ* SERS from a single nanoparticle assembly, a 660 nm DPSS laser (Laser Quantum, OPS 1500−1.5 W) was expanded with a 5× beam expander and focused onto the plasmonic substrate with a 40× objective (Nikon, NA 0.75) in the inverted microscope. *In situ* SERS was conducted on multiple nanoparticle assemblies by adding an SLM (Hamamatsu, X13138-01) and two relay lenses (focal lengths of 100 and 30 cm, respectively) in the original optical path.

Computational Fluid Dynamics Simulations. Finite element method numerical simulations (COMSOL Multiphysics) were employed to analyze the temperature distribution around the laser beam focused at the substrate−water interface. For simplicity, a 2D axisymmetric model composed of a glass substrate, AuNT assembly, and water was established. Since the physics involved heat transfer in solids (glass substrate and AuNT assembly) and fluids, the predefined model conjugate heat transfer was used. A Gaussian distribution heat source was placed at the substrate−fluid interface to model the heating from the laser beam. For cases with AuNTs sandwiched between the substrate and the fluid layer, a highly conductive layer was used to model heat transfer in the AuNT layer. Room temperature was set at all other boundaries.

ASSOCIATED CONTENT

Supporting Information

The Supporting Information is available free of charge on the ACS Publications website at DOI: 10.1021/acsnano.6b05486.

Optical properties of the plasmonic nanoparticle suspensions (Figure S1), transmission electron spectroscopy of AuNTs (Figure S2), structural and optical properties of plasmonic substrates (Figure S3), optical-power dependence of AuNT assembly formation (Figure S4), AuNS and AgNS assembly (Figure S5), Raman spectrum of rhodamine 6G measured with a single AuNS assembly (Figure S6), SERS with multiple plasmonic nanoparticle assemblies (Figure S7), and Raman spectra of methyl orange (Figure S8) (PDF)

Movie 1: Assembly process of AuNTs (AVI)

Movie 2: Redispersion of an AuNT assembly (AVI)

Movie 3: Delivery of a stable nanoparticle assembly from AuNIs to a glass substrate (AVI)

Movie 4: Dynamic manipulation of multiple AuNT assemblies (AVI)

AUTHOR INFORMATION

Corresponding Author

*E-mail: zheng@austin.utexas.edu.

Author Contributions

□L. Lin and X. Peng contributed equally to this paper.

Notes

The authors declare no competing financial interest.

ACKNOWLEDGMENTS

The authors acknowledge the financial support of the Beckman Young Investigator Program and the Texas Advanced Computing Center (TACC) at The University of Texas at Austin for providing HPC resources that have contributed to the research results reported in this paper. URL: http://www.tacc.utexas.edu. M.B. acknowledges support from the Jack Kilby/Texas Instruments Endowed Faculty Fellowship in Computer Engineering. L.M.L.-M. acknowledges funding from the Spanish Ministerio de Economíay Competitividad MINECO (Grant No. MAT2013-46101-R) and the European Research Council (ERC Advanced Grant No. 267867, PLASMAQUO).

REFERENCES

(1) Halas, N. J.; Lal, S.; Chang, W. S.; Link, S.; Nordlander, P. Plasmons in Strongly Coupled Metallic Nanostructures. *Chem. Rev.* **2011**, *111*, 3913−3961.

(2) Hoang, T. B.; Akselrod, G. M.; Argyropoulos, C.; Huang, J.; Smith, D. R.; Mikkelsen, M. H. Ultrafast Spontaneous Emission Source Using Plasmonic Nanoantennas. *Nat. Commun.* **2015**, *6*, 7788.

(3) Lee, B.; Park, J.; Han, G. H.; Ee, H.-S.; Naylor, C. H.; Liu, W.; Johnson, A. T. C.; Agarwal, R. Fano Resonance and Spectrally Modified Photoluminescence Enhancement in Monolayer MoS_2 Integrated with Plasmonic Nanoantenna Array. *Nano Lett.* **2015**, *15*, 3646−3653.

(4) Chikkaraddy, R.; de Nijs, B.; Benz, F.; Barrow, S. J.; Scherman, O. A.; Rosta, E.; Demetriadou, A.; Fox, P.; Hess, O.; Baumberg, J. J. Single-Molecule Strong Coupling at Room Temperature in Plasmonic Nanocavities. *Nature* **2016**, *535*, 127−130.

(5) Zhu, Z.; Liu, W.; Li, Z.; Han, B.; Zhou, Y.; Gao, Y.; Tang, Z. Manipulation of Collective Optical Activity in One-Dimensional Plasmonic Assembly. *ACS Nano* **2012**, *6*, 2326−2332.

(6) Liu, W.; Zhu, Z.; Deng, K.; Li, Z.; Zhou, Y.; Qiu, H.; Gao, Y.; Che, S.; Tang, Z. Gold Nanorod@Chiral Mesoporous Silica Core−Shell Nanoparticles with Unique Optical Properties. *J. Am. Chem. Soc.* **2013**, *135*, 9659−9664.

(7) Stamplecoskie, K. G.; Scaiano, J. C.; Tiwari, V. S.; Anis, H. Optimal Size of Silver Nanoparticles for Surface-Enhanced Raman Spectroscopy. *J. Phys. Chem. C* **2011**, *115*, 1403−1409.

(8) Mock, J. J.; Barbic, M.; Smith, D. R.; Schultz, D. A.; Schultz, S. Shape Effects in Plasmon Resonance of Individual Colloidal Silver Nanoparticles. *J. Chem. Phys.* **2002**, *116*, 6755−6759.

(9) Motl, N. E.; Smith, A. F.; DeSantis, C. J.; Skrabalak, S. E. Engineering Plasmonic Metal Colloids through Composition and Structural Design. *Chem. Soc. Rev.* **2014**, *43*, 3823−3834.

(10) Su, K. H.; Wei, Q. H.; Zhang, X.; Mock, J. J.; Smith, D. R.; Schultz, S. Interparticle Coupling Effects on Plasmon Resonances of Nanogold Particles. *Nano Lett.* **2003**, *3*, 1087−1090.

(11) Zhu, Z.; Meng, H.; Liu, W.; Liu, X.; Gong, J.; Qiu, X.; Jiang, L.; Wang, D.; Tang, Z. Superstructures and SERS Properties of Gold

DOI: 10.1021/acsnano.6b05486
ACS Nano XXXX, XXX, XXX−XXX

Nanocrystals with Different Shapes. *Angew. Chem., Int. Ed.* **2011**, *50*, 1593−1596.
(12) Patra, P. P.; Chikkaraddy, R.; Tripathi, R. P. N.; Dasgupta, A.; Kumar, G. V. P. Plasmofluidic Single-Molecule Surface-Enhanced Raman Scattering from Dynamic Assembly of Plasmonic Nanoparticles. *Nat. Commun.* **2014**, *5*, 4357.
(13) Fazio, B.; D'Andrea, C.; Foti, A.; Messina, E.; Irrera, A.; Donato, M. G.; Villari, V.; Micali, N.; Maragò, O. M.; Gucciardi, P. G. SERS Detection of Biomolecules at Physiological pH *via* Aggregation of Gold Nanorods Mediated by Optical Forces and Plasmonic Heating. *Sci. Rep.* **2016**, *6*, 26952.
(14) Ye, J.; Wen, F.; Sobhani, H.; Lassiter, J. B.; Dorpe, P. V.; Nordlander, P.; Halas, N. J. Plasmonic Nanoclusters: Near Field Properties of the Fano Resonance Interrogated with SERS. *Nano Lett.* **2012**, *12*, 1660−1667.
(15) Taladriz-Blanco, P.; Buurma, N. J.; Rodriguez-Lorenzo, L.; Perez-Juste, J.; Liz-Marzan, L. M.; Herves, P. Reversible Assembly of Metal Nanoparticles Induced by Penicillamine. Dynamic Formation of SERS Hot Spots. *J. Mater. Chem.* **2011**, *21*, 16880−16887.
(16) Li, W.; Kanyo, I.; Kuo, C.-H.; Thanneeru, S.; He, J. Ph-Programmable Self-Assembly of Plasmonic Nanoparticles: Hydrophobic Interaction *versus* Electrostatic Repulsion. *Nanoscale* **2015**, *7*, 956−964.
(17) Li, Z.; Zhu, Z.; Liu, W.; Zhou, Y.; Han, B.; Gao, Y.; Tang, Z. Reversible Plasmonic Circular Dichroism of Au Nanorod and DNA Assemblies. *J. Am. Chem. Soc.* **2012**, *134*, 3322−3325.
(18) Liu, Y.; Han, X.; He, L.; Yin, Y. Thermoresponsive Assembly of Charged Gold Nanoparticles and Their Reversible Tuning of Plasmon Coupling. *Angew. Chem., Int. Ed.* **2012**, *51*, 6373−6377.
(19) Si, S.; Raula, M.; Paira, T. K.; Mandal, T. K. Reversible Self-Assembly of Carboxylated Peptide-Functionalized Gold Nanoparticles Driven by Metal-Ion Coordination. *ChemPhysChem* **2008**, *9*, 1578−1584.
(20) Su, B.; Abid, J.-P.; Fermín, D. J.; Girault, H. H.; Hoffmannová, H.; Krtil, P.; Samec, Z. Reversible Voltage-Induced Assembly of Au Nanoparticles at Liquid|Liquid Interfaces. *J. Am. Chem. Soc.* **2004**, *126*, 915−919.
(21) Klajn, R.; Bishop, K. J. M.; Grzybowski, B. A. Light-Controlled Self-Assembly of Reversible and Irreversible Nanoparticle Supra-structures. *Proc. Natl. Acad. Sci. U. S. A.* **2007**, *104*, 10305−10309.
(22) Kundu, P. K.; Samanta, D.; Leizrowice, R.; Margulis, B.; Zhao, H.; Börner, M.; Udayabhaskararao, T.; Manna, D.; Klajn, R. Light-Controlled Self-Assembly of Non-Photoresponsive Nanoparticles. *Nat. Chem.* **2015**, *7*, 646−652.
(23) Bao, Y.; Yan, Z.; Scherer, N. F. Optical Printing of Electrodynamically Coupled Metallic Nanoparticle Arrays. *J. Phys. Chem. C* **2014**, *118*, 19315−19321.
(24) Yan, Z.; Sajjan, M.; Scherer, N. F. Fabrication of a Material Assembly of Silver Nanoparticles Using the Phase Gradients of Optical Tweezers. *Phys. Rev. Lett.* **2015**, *114*, 143901.
(25) Gargiulo, J.; Cerrota, S.; Cortés, E.; Violi, I. L.; Stefani, F. D. Connecting Metallic Nanoparticles by Optical Printing. *Nano Lett.* **2016**, *16*, 1224−1229.
(26) Urban, A. S.; Lutich, A. A.; Stefani, F. D.; Feldmann, J. Laser Printing Single Gold Nanoparticles. *Nano Lett.* **2010**, *10*, 4794−4798.
(27) Nedev, S.; Urban, A. S.; Lutich, A. A.; Feldmann, J. Optical Force Stamping Lithography. *Nano Lett.* **2011**, *11*, 5066−5070.
(28) Guffey, M. J.; Scherer, N. F. All-Optical Patterning of Au Nanoparticles on Surfaces Using Optical Traps. *Nano Lett.* **2010**, *10*, 4302−4308.
(29) Kyrsting, A.; Bendix, P. M.; Stamou, D. G.; Oddershede, L. B. Heat Profiling of Three-Dimensionally Optically Trapped Gold Nanoparticles Using Vesicle Cargo Release. *Nano Lett.* **2011**, *11*, 888−892.
(30) Brown, S. D.; Nativo, P.; Smith, J.-A.; Stirling, D.; Edwards, P. R.; Venugopal, B.; Flint, D. J.; Plumb, J. A.; Graham, D.; Wheate, N. J. Gold Nanoparticles for the Improved Anticancer Drug Delivery of the Active Component of Oxaliplatin. *J. Am. Chem. Soc.* **2010**, *132*, 4678−4684.
(31) Tong, L.; Righini, M.; Gonzalez, M. U.; Quidant, R.; Kall, M. Optical Aggregation of Metal Nanoparticles in a Microfluidic Channel for Surface-Enhanced Raman Scattering Analysis. *Lab Chip* **2009**, *9*, 193−195.
(32) Messina, E.; Cavallaro, E.; Cacciola, A.; Saija, R.; Borghese, F.; Denti, P.; Fazio, B.; D'Andrea, C.; Gucciardi, P. G.; Iatì, M. A.; Meneghetti, M.; Compagnini, G.; Amendola, V.; Maragò, O. M. Manipulation and Raman Spectroscopy with Optically Trapped Metal Nanoparticles Obtained by Pulsed Laser Ablation in Liquids. *J. Phys. Chem. C* **2011**, *115*, 5115−5122.
(33) Stetciura, I. Y.; Yashchenok, A.; Masic, A.; Lyubin, E. V.; Inozemtseva, O. A.; Drozdova, M. G.; Markvichova, E. A.; Khlebtsov, B. N.; Fedyanin, A. A.; Sukhorukov, G. B.; Gorin, D. A.; Volodkin, D. Composite SERS-Based Satellites Navigated by Optical Tweezers for Single Cell Analysis. *Analyst* **2015**, *140*, 4981−4986.
(34) Svedberg, F.; Li, Z.; Xu, H.; Käll, M. Creating Hot Nanoparticle Pairs for Surface-Enhanced Raman Spectroscopy through Optical Manipulation. *Nano Lett.* **2006**, *6*, 2639−2641.
(35) Yoshikawa, H.; Matsui, T.; Masuhara, H. Reversible Assembly of Gold Nanoparticles Confined in an Optical Microcage. *Phys. Rev. E* **2004**, *70*, 061406.
(36) González-Rubio, G.; Guerrero-Martínez, A.; Liz-Marzán, L. M. Reshaping, Fragmentation, and Assembly of Gold Nanoparticles Assisted by Pulse Lasers. *Acc. Chem. Res.* **2016**, *49*, 678−686.
(37) González-Rubio, G.; González-Izquierdo, J.; Bañares, L.; Tardajos, G.; Rivera, A.; Altantzis, T.; Bals, S.; Peña-Rodríguez, O.; Guerrero-Martínez, A.; Liz-Marzán, L. M. Femtosecond Laser-Controlled Tip-to-Tip Assembly and Welding of Gold Nanorods. *Nano Lett.* **2015**, *15*, 8282−8288.
(38) Braun, M.; Cichos, F. Optically Controlled Thermophoretic Trapping of Single Nano-Objects. *ACS Nano* **2013**, *7*, 11200−11208.
(39) Braun, M.; Wurger, A.; Cichos, F. Trapping of Single Nano-Objects in Dynamic Temperature Fields. *Phys. Chem. Chem. Phys.* **2014**, *16*, 15207−15213.
(40) Ilic, O.; Kaminer, I.; Lahini, Y.; Buljan, H.; Soljačić, M. Exploiting Optical Asymmetry for Controlled Guiding of Particles with Light. *ACS Photonics* **2016**, *3*, 197−202.
(41) Thamdrup, L. H.; Larsen, N. B.; Kristensen, A. Light-Induced Local Heating for Thermophoretic Manipulation of DNA in Polymer Micro- and Nanochannels. *Nano Lett.* **2010**, *10*, 826−832.
(42) Reichl, M.; Herzog, M.; Götz, A.; Braun, D. Why Charged Molecules Move across a Temperature Gradient: The Role of Electric Fields. *Phys. Rev. Lett.* **2014**, *112*, 198101.
(43) Braun, M.; Bregulla, A. P.; Günther, K.; Mertig, M.; Cichos, F. Single Molecules Trapped by Dynamic Inhomogeneous Temperature Fields. *Nano Lett.* **2015**, *15*, 5499−5505.
(44) Scarabelli, L.; Coronado-Puchau, M.; Giner-Casares, J. J.; Langer, J.; Liz-Marzán, L. M. Monodisperse Gold Nanotriangles: Size Control, Large-Scale Self-Assembly, and Performance in Surface-Enhanced Raman Scattering. *ACS Nano* **2014**, *8*, 5833−5842.
(45) Jin, R.; Cao, Y.; Mirkin, C. A.; Kelly, K. L.; Schatz, G. C.; Zheng, J. G. Photoinduced Conversion of Silver Nanospheres to Nanoprisms. *Science* **2001**, *294*, 1901−1903.
(46) Pignolet, C.; Euvrard, M.; Foissy, A.; Filiâtre, C. Electro-deposition of Latex Particles in the Presence of Surfactant: Investigation of Deposit Morphology. *J. Colloid Interface Sci.* **2010**, *349*, 41−48.
(47) Gómez-Graña, S.; Hubert, F.; Testard, F.; Guerrero-Martínez, A.; Grillo, I.; Liz-Marzán, L. M.; Spalla, O. Surfactant (Bi)Layers on Gold Nanorods. *Langmuir* **2012**, *28*, 1453−1459.
(48) Würger, A. Transport in Charged Colloids Driven by Thermoelectricity. *Phys. Rev. Lett.* **2008**, *101*, 108302.
(49) Bregulla, A. P.; Würger, A.; Günther, K.; Mertig, M.; Cichos, F. Thermo-Osmotic Flow in Thin Films. *Phys. Rev. Lett.* **2016**, *116*, 188303.
(50) Movchan, T. G.; Soboleva, I. V.; Plotnikova, E. V.; Shchekin, A. K.; Rusanov, A. I. Dynamic Light Scattering Study of Cetyltrimethylammonium Bromide Aqueous Solutions. *Colloid J.* **2012**, *74*, 239−247.

DOI: 10.1021/acsnano.6b05486
ACS Nano XXXX, XXX, XXX−XXX

(51) Würger, A. Thermal Non-Equilibrium Transport in Colloids. *Rep. Prog. Phys.* **2010**, *73*, 126601.
(52) Lin, L.; Peng, X.; Mao, Z.; Li, W.; Yogeesh, M. N.; Rajeeva, B. B.; Perillo, E. P.; Dunn, A. K.; Akinwande, D.; Zheng, Y. Bubble-Pen Lithography. *Nano Lett.* **2016**, *16*, 701−708.
(53) Nie, S.; Emory, S. R. Probing Single Molecules and Single Nanoparticles by Surface-Enhanced Raman Scattering. *Science* **1997**, *275*, 1102−1106.
(54) Campion, A.; Kambhampati, P. Surface-Enhanced Raman Scattering. *Chem. Soc. Rev.* **1998**, *27*, 241−250.
(55) Kneipp, K.; Wang, Y.; Kneipp, H.; Perelman, L. T.; Itzkan, I.; Dasari, R. R.; Feld, M. S. Single Molecule Detection Using Surface-Enhanced Raman Scattering (SERS). *Phys. Rev. Lett.* **1997**, *78*, 1667−1670.
(56) Stiles, P. L.; Dieringer, J. A.; Shah, N. C.; Duyne, R. P. V. Surface-Enhanced Raman Spectroscopy. *Annu. Rev. Anal. Chem.* **2008**, *1*, 601−626.
(57) Garcia-Leis, A.; Garcia-Ramos, J. V.; Sanchez-Cortes, S. Silver Nanostars with High SERS Performance. *J. Phys. Chem. C* **2013**, *117*, 7791−7795.
(58) McLellan, J. M.; Li, Z.-Y.; Siekkinen, A. R.; Xia, Y. The SERS Activity of a Supported Ag Nanocube Strongly Depends on Its Orientation Relative to Laser Polarization. *Nano Lett.* **2007**, *7*, 1013−1017.
(59) Wang, H.; Levin, C. S.; Halas, N. J. Nanosphere Arrays with Controlled Sub-10-nm Gaps as Surface-Enhanced Raman Spectroscopy Substrates. *J. Am. Chem. Soc.* **2005**, *127*, 14992−14993.
(60) Lim, D.-K.; Jeon, K.-S.; Hwang, J.-H.; Kim, H.; Kwon, S.; Suh, Y. D.; Nam, J.-M. Highly Uniform and Reproducible Surface-Enhanced Raman Scattering from DNA-Tailorable Nanoparticles with 1-nm Interior Gap. *Nat. Nanotechnol.* **2011**, *6*, 452−460.
(61) Chen, S.; Meng, L.-Y.; Shan, H.-Y.; Li, J.-F.; Qian, L.; Williams, C. T.; Yang, Z.-L.; Tian, Z.-Q. How to Light Special Hot Spots in Multiparticle−Film Configurations. *ACS Nano* **2015**, *10*, 581−587.
(62) Shams Mousavi, S. H.; Eftekhar, A. A.; Atabaki, A. H.; Adibi, A. Band-Edge Bilayer Plasmonic Nanostructure for Surface Enhanced Raman Spectroscopy. *ACS Photonics* **2015**, *2*, 1546−1551.
(63) Li, W.; Camargo, P. H. C.; Lu, X.; Xia, Y. Dimers of Silver Nanospheres: Facile Synthesis and Their Use as Hot Spots for Surface-Enhanced Raman Scattering. *Nano Lett.* **2009**, *9*, 485−490.
(64) Hildebrandt, P.; Stockburger, M. Surface-Enhanced Resonance Raman Spectroscopy of Rhodamine 6G Adsorbed on Colloidal Silver. *J. Phys. Chem.* **1984**, *88*, 5935−5944.
(65) Kreibig, U.; Vollmer, M. *Optical Properties of Metal Clusters*; Springer: Berlin, 1995.

DOI: 10.1021/acsnano.6b05486
ACS Nano XXXX, XXX, XXX−XXX